Manipulation of Particles In Two Dimensions Using Phase Controllable Ultrasonic Standing Waves

C. R. P. Courtney[1], C.-K. Ong[1], B. W. Drinkwater[1], A. L. Bernassau[2], P. D. Wilcox[1], D. R. S. Cumming[2]

[1]*Department of Mechanical Engineering, University of Bristol, Bristol BS8 1TR, United Kingdom*
[2]*Electronics & Electrical Engineering Rankine Building, University of Glasgow, Glasgow G12 8LT, United Kingdom*

The ability to manipulate dense micrometer-scale objects in fluids is of interest to biosciences with a view to improving analysis techniques and enabling tissue engineering. A method of trapping micrometer-scale particles and manipulating them on a two-dimensional plane is proposed and demonstrated. Phase-controlled counter-propagating waves are used to generate ultrasonic standing waves with arbitrary nodal positions. The acoustic radiation force drives dense particles to pressure nodes. It is shown analytically that a series of point-like traps can be produced in a two-dimensional plane using two orthogonal pairs of counter-propagating waves. These traps can be manipulated by appropriate adjustment of the relative phases. Four 5-MHz transducers (designed to minimize reflection) are used as sources of counter-propagating waves in a water-filled cavity. 10-μm-diameter polystyrene beads are trapped and manipulated. The relationship between trapped particle positions and the relative phases of the four transducers is measured and shown to agree with analytically derived expressions. The force available is measured by determining the response to a sudden change in field and found to be 30 pN, for a 30 V_{pp} input, which is in agreement with the predictions of models of the system. A scalable fabrication approach to producing devices is demonstrated.

Key words: Ultrasonics, Acoustic Radiation Force, Particle Manipulation.

1. Introduction

The force applied to micrometer scale objects as a result of interaction with ultrasonic waves offers opportunities for application in the biosciences. Generally standing waves, generated in resonant cavities, have attracted the most interest, as they produce greater forces, however the dexterity of these devices is limited by the strong correlation of the acoustic field shape to the device geometry. In this paper a method of using counter-propagating waves to generate standing-wave patterns is developed. This allows pressure nodes, which act to trap dense particles, to be moved by varying the phase relationships between exciting transducers. The work builds on previous work, which used a pair of transducers for one-dimensional manipulation (Courtney et al., 2010), by using two opposing pairs of transducers, positioned orthogonally, in order to trap and manipulate particles in two dimensions.

Proc. R. Soc. A 1–27; doi: 10.1098/rspa.00000000
29 April 2011

Although practical applications are only just being explored, the acoustic radiation force has been of academic interest for many years: Kundt (1868) demonstrated the effect using cork dust in a glass tube in the 19th century and King (1934) provided analytical solutions for the force on an incompressible sphere in an inviscid fluid under the influence of standing or travelling waves. This analysis relied on the particle diameter being substantially smaller than the incident wavelength. Further development of this analysis produced solutions for compressible spheres (Yosioka & Kawasima, 1955; Gor'kov, 1962), still in inviscid fluids. More extensive calculations, to include viscosity and heat conductivity, have been performed (Doinikov, 1994, 1997; Mitri, 2009). However the effects of these factors are only appreciable where travelling waves are involved (Doinikov, 1996), rather than standing waves, so for most devices developed to date the results due to Gor'kov (1962) and Yosioka & Kawasima (1955) are suitable for calculating the forces involved.

Trapping particles with megahertz-frequency standing waves has been used to agglomerate cells allowing filtering of cells from fluids by sedimentation or enhancement of bead based assays (Coakley, 1997; Coakley et al., 2000). Ultrasonic standing waves have been used to guide particles suspended in a fluid undergoing laminar flow in devices with split inlets and/or outlets. This allows the division of particles from fluid, for concentration, filtration (Yasuda et al., 1995) or the sorting of particles (Johnson & Feke, 1995). These approaches have been developed, primarily in the area of micro-scale devices, and the field of manipulating micro-particles (and in particular cells) is reviewed by Laurell et al. (2007) and appears in a general review of separation techniques using continuous flow by Pamme (2007). In addition to applications in the biosciences there has been interest in using the acoustic radiation force in the production of acoustic metamaterials. Saito et al. (1998) demonstrated the construction of a structured composite material consisting of 10-μm-diameter acrylic spheres trapped in layers in a epoxy solution which was then cured. The same authors extended this approach by using two pairs of transducers arranged orthogonally to produce a grid pattern (Saito et al., 1999). Pairs of transducers were used to improve field uniformity and not, as in the current work, to introduce a manipulation capability. Mitri et al. (2011) demonstrated the construction of such a material by using opposing transducers to trap layers of diamond nanoparticles in liquid epoxy, which were fixed in position as the epoxy cured.

A recent development in the field of micro-particle manipulation is the use of surface acoustic waves (SAWs) generated using interdigital transducers (IDTs) on lithium niobate substrates to generate acoustic fields in fluid-filled cavities and trap particles. Wood et al. (2008) used opposing interdigital transducers to trap 0.5 to 2-μm diameter particles in lines in a 25-μm deep channel. Trapping of particles in a grid-pattern using SAWs has been demonstrated using two pairs of IDTs arranged orthogonally (Wood et al., 2009) and using two IDTs at right angles, but without opposing IDTs (Shi et al., 2009). By varying the excitation frequency Wood et al. (2008, 2009) showed particle manipulation over distances of 5 μm.

The above techniques have almost exclusively concentrated on acoustic fields defined by the geometry of the system, which drive particles to particular points in the fluid cavity. However, there has also been interest in increasing versatility by using devices that can generate variable fields to allow a more generalized

manipulation of particles. There are currently four approaches to manipulating particles: mode switching, 'acoustical tweezers', linear arrays and counter-propagating waves. Trinh *et al.* used frequency switching between resonant standing waves to levitate and manoeuvre, in one dimension, hollow quartz spheres in air (Trinh et al., 1986). Work by Min *et al.* with Styrofoam spheres used a similar approach, but added the concept of trapping in a node of a particular mode, switching the excitation off to allow the particle to drop slightly before pulsing the excitation at that mode to provide a momentum kick, thus allowing the particle to be trapped in another mode by applying an excitation at a different frequency at an appropriate time (Min et al., 1992). Another recent variation on this approach uses switching between two modes (a half wavelength and a quarter wavelength respectively) to force particles to an equilibrium position between the nodes of the two modes (Glynne-Jones et al., 2010). Focused ultrasonic beams have been used in a manner analogous to optical tweezers (Wu & Du, 1990; Wu, 1991) by trapping latex particles with a diameter of 270 μm using 3.5 MHz ultrasonic fields. Initially these 'acoustical tweezers' used opposing focused transducers to produce a trap at their, common, focal point (Wu, 1991). More recent theoretical (Lee et al., 2005; Lee & Shung, 2006) and experimental (Lee et al., 2009) work has demonstrated the feasibility of using a single focused transducer working at high frequency (30 MHz) to trap particles much larger than a wavelength in diameter against a surface. Particle manipulation has been achieved by moving the transducer and hence the focal position. An approach which could be used for manipulation in a similar manner was proposed and demonstrated by Yamakoshi & Noguchi (1998): two curved piezoelectric plates were placed next to each other with a common centre of curvature and driven out of phase resulting in a field with a node along the axis perpendicular to the centre of the pair of plates and antinodes either side, allowing 30μm-diameter polystyrene spheres to be trapped against a fluid flow perpendicular to the node. Recent theoretical work suggests that the versatility of acoustic tweezers may be improved by the use of Bessel beams (Marston, 2006; Mitri, 2008). The third method of manoeuvring particles using the acoustic radiation field uses a linear array of transducers placed opposite a reflector. Simultaneously exciting 3 adjacent array elements allows a standing wave to be generated above those elements, which is sufficient to levitate the target particles (80 μm alumina powder) and leads to particles trapped at the nodes of the field over the active elements. By switching elements it is possible to smoothly move the region of activity and hence move the trapped particles along the array (Kozuka et al., 1996). This technique was further improved by using focussed transducers to improve the trapping and adding frequency switching to allow some control perpendicular to the trap positions (Kozuka et al., 1998a). Recently work has been done on moving from large (10s of millimetre) devices to microfluidic devices, with 10-μm-diameter polystyrene beads being successfully manipulated in a 300-μm channel, using a linear array (Demore et al., 2010).

The fourth approach to particle manipulation, which is exploited in this paper, involves generating a standing wave as the sum of two independently-generated travelling waves. Using such a standing wave (rather than one generated by resonance) allows the nodal positions of the field to be changed by varying the relative phase of the two sources. The difficulty is generating opposing travelling waves without generating resonant standing waves. The first implementation of this method worked by using transducers in a large water tank and inclining

the transducers slightly (15^o) so that their beams intersected, but there was no reflection from the front faces of the opposing transducer (Kozuka et al., 1998b). Haake & Dual (2002) showed analytically that the position of the pressure nodes in a fluid between two piezoelectric plates could be varied as a function of the relative phase between the voltages applied to the plates. However they indicated that controlled positioning would not be possible at certain points due to interference. An alternative implementation of this principle was used by the current authors to manipulate 10-Îijm-diameter polystyrene particles in one dimension, by using transducers acoustically matched to the fluid with an absorbing backing to prevent reflections leading to resonant modes, and demonstrated that the particles could be trapped and moved arbitrary distances (Courtney et al., 2010). This approach removed the need to work in a large chamber (as would be required for the approach of Kozuka et al. (1998b)) and is extended to motion in two dimensions in this paper.

The use of counter-propagating waves for particle manipulation has the advantage of allowing dexterous manipulation, without being limited by fixed nodal positions, with a monotonic relationship between relative phase an particle position. The absence of resonances in the system allows for rapid changes in the field even in chambers that are tens of wavelengths in size and avoids potential problems with the trapping of large numbers of particles leading to a change in the resonant frequency of the device (as observed by Kwiatkowski & Marston (1998)). Operation in a narrow frequency band allows transducer optimization, taking advantage of the high Q values of piezoceramics. The use of matched transducers, positioned around the periphery of the fluid chamber allows the use of relatively small chambers (rather than large tanks), whilst allowing access from above for handling, observation or optical tweezing.

The paper starts with an analytical section deriving the relationship between phase and nodal position for a pair of counter-propagating waves and the shapes of traps produced by two orthogonal pairs of counter-propagating devices (section 3). This is followed by a description of the device designed to demonstrate the approach (section 4). Two models are then described, a one dimensional electro-acoustic model used to optimize the design of the transducers required and a two-dimensional finite element model used to predict the field shape and pressure amplitude in the device (section 5). The experimental results section demonstrates the manipulation of particles by the device, and the relationship between phase and particle position (section 6). This section includes the estimation of the force applied to a particle by measurement of the response to a sudden shift in the applied field. Finally a scalable fabrication method is proposed and results showing its viability are presented (section 7).

2. Radiation force

The acoustic radiation force acting on a small compressible sphere in an inviscid fluid was first calculated by Yosioka & Kawasima (1955), and developed into a more convenient potential function by Gor'kov (1962). Gor'kov writes the force, F, in terms of a potential U, such that

$$\mathbf{F} = -\nabla U. \tag{2.1}$$

The potential for a spherical particle of radius, a, density ρ_0 and bulk modulus K_0 in a fluid of density ρ, bulk modulus K and bulk sound velocity $c = \sqrt{K/\rho}$ is given by

$$U = 2\pi a^3 \rho \left\{ \frac{\overline{p_{in}^2}}{3\rho^2 c^2} f_1 - \frac{\overline{v^2}}{2} f_2 \right\}, \tag{2.2}$$

where $\overline{p_{in}^2}$ is the mean square pressure of the incident wave at the particle position and $\overline{v^2}$ the mean squared velocity. The calculation is valid for particles with radius substantially smaller than one wavelength in the fluid ($a << \lambda$) and for arbitrary fields, provided that they are not purely travelling waves (Gor'kov, 1962). The factors f_1 and f_2 depend on the relative densities and sound speeds of the spheres and fluids and are given by:

$$f_1 = 1 - \frac{K}{K_0}$$
$$f_2 = 2\frac{(\rho_0 - \rho)}{2\rho_0 + \rho}. \tag{2.3}$$

3. Counter-propagating wave method

The method of trapping and manipulating particles used in this paper relies on the principle that a standing wave can be generated as a superposition of two counter propagating waves and that, by varying the phase difference between the counter-propagating waves, it is possible to move the nodal positions of the resultant standing wave. In order to generate the two waves, opposing transducers, matched to prevent reflection at the front surface and backed to absorb energy, are used. A one dimensional propagation analysis is used to demonstrate the principle and calculate the relationship between position, acoustic pressure and phase.

(*a*) *Principle of particle control in one dimension*

Consider a one dimensional linear system consisting of two opposing transducers, one positioned at $x = -x_0$ and one at $x = x_0$. If each transducer has a reflection coefficient R, and secondary reflections can be ignored, then the resultant field, P_1, in the region $-x_0 \leq x \leq x_0$ due to the transducer at $-x_0$ can be written as the superposition of the wave travelling away from the activated transducer, which has amplitude, P_0, and the reflected part, amplitude $P_0 R$:

$$\begin{aligned} P_1(x,t) &= P_0 \left[e^{ik(x+x_0)} + Re^{-ik(x-3x_0)} \right] e^{-i\omega t} \\ &= P_0 e^{ikx_0} \left[2\cos\,(kx) + \left(Re^{i2kx_0} - 1 \right) e^{-ikx} \right] e^{-i\omega t}. \end{aligned} \tag{3.1}$$

The field for the transducer at $+x_0$ is

$$\begin{aligned} P_2(x,t) &= P_0 \left[e^{-ik(x-x_0)} + Re^{ik(x+3x_0)} \right] e^{-i\omega t} \\ &= P_0 e^{ikx_0} \left[2\cos\,(kx) + \left(Re^{i2kx_0} - 1 \right) e^{ikx} \right] e^{-i\omega t}. \end{aligned} \tag{3.2}$$

Dropping the time dependence term ($e^{-i\omega t}$), and introducing an arbitrary phase difference of $\Delta\phi$ between the two excitations, the total field when both transducers are excited is

$$\begin{aligned} P(x) &= P_1 e^{i\Delta\phi/2} + P_2 e^{-i\Delta\phi/2} \\ &= 2P_0 e^{ikx_0}\left[2\cos(kx)\cos\left(\frac{\Delta\phi}{2}\right) + \left(Re^{i2kx_0} - 1\right)\cos\left(kx - \frac{\Delta\phi}{2}\right)\right] \end{aligned} \tag{3.3}$$

Figure 1(a) shows the behaviour of the pressure field as a function of the phase change for $R = 0.2$ and $x_0 = 3\lambda$, note that the effect of the non-zero reflection coefficient is to introduce a deviation from the linear relation between position of the nodes and phase and introduce a variation in the anti-node amplitude with phase. Both these can be evaluated from equation 3.3. The locus of the minimum value of $P(x)$, calculated from eq. 3.3, varies as:

$$\Delta x = \frac{1}{k}\arctan\left[\left(\frac{R\cos(2kx_0) - 1}{R\cos(2kx_0) + 1}\right)\tan\left(\frac{\Delta\phi}{2}\right)\right]. \tag{3.4}$$

Note that this has a similar form to the zero-pressure position predicted for such a system with only single transducer activated (see equation (18) of Haake & Dual (2002)), however unlike the single transducer case, in the two transducer system the nodal positions depend on the relative phase and do not vary in time unless the relative phase is changed. For the case where the reflection coefficient is non-zero, the anti-node has a maximum value when $\Delta\phi = 0$ of $2P_0\cos(kx_0)(1 + R\cos(2kx_0))$, however the amplitude drops to $2P_0\cos(kx_0)(1 - R\cos(2kx_0))$ for $\Delta\phi = \pi$ (i.e. when trapping the particles at a distance $\lambda/2$ from the $\Delta\phi = 0$ trap). So there is a reduction of up to a ratio of $\frac{(1-R\cos(2kx_0))}{(1+R\cos(2kx_0))}$ depending on the preferred trapping position. In principle the effect of reflection could be removed by ensuring that $\cos(2kx_0) = 0$, which is the case when the transducer separation, $2x_0$, is an odd number of quarter wavelengths. However, this is difficult in practice, where there are many wavelengths across the fluid chamber, and minimizing reflection is the best way of ensuring consistent traps and good positional control.

(*b*) *Principle of particle control in two dimensions*

In order to elucidate how a trap can be created in two dimensions using two pairs of transducers, consider an idealized case where there is no reflection and each transducer produces a plane travelling wave. In the absence of reflection the transducer position is unimportant and so the effect of transducer position is included in phase delays. Omitting the harmonic time dependence and the contribution from each transducer can be written:

$$\begin{aligned} P_1(x,y) &= P_0\exp\left[i(kx + \phi_1)\right] \\ P_2(x,y) &= P_0\exp\left[i(-kx + \phi_2)\right] \\ P_3(x,y) &= P_0\exp\left[i(ky + \phi_3)\right] \\ P_4(x,y) &= P_0\exp\left[i(-ky + \phi_4)\right]. \end{aligned} \tag{3.5}$$

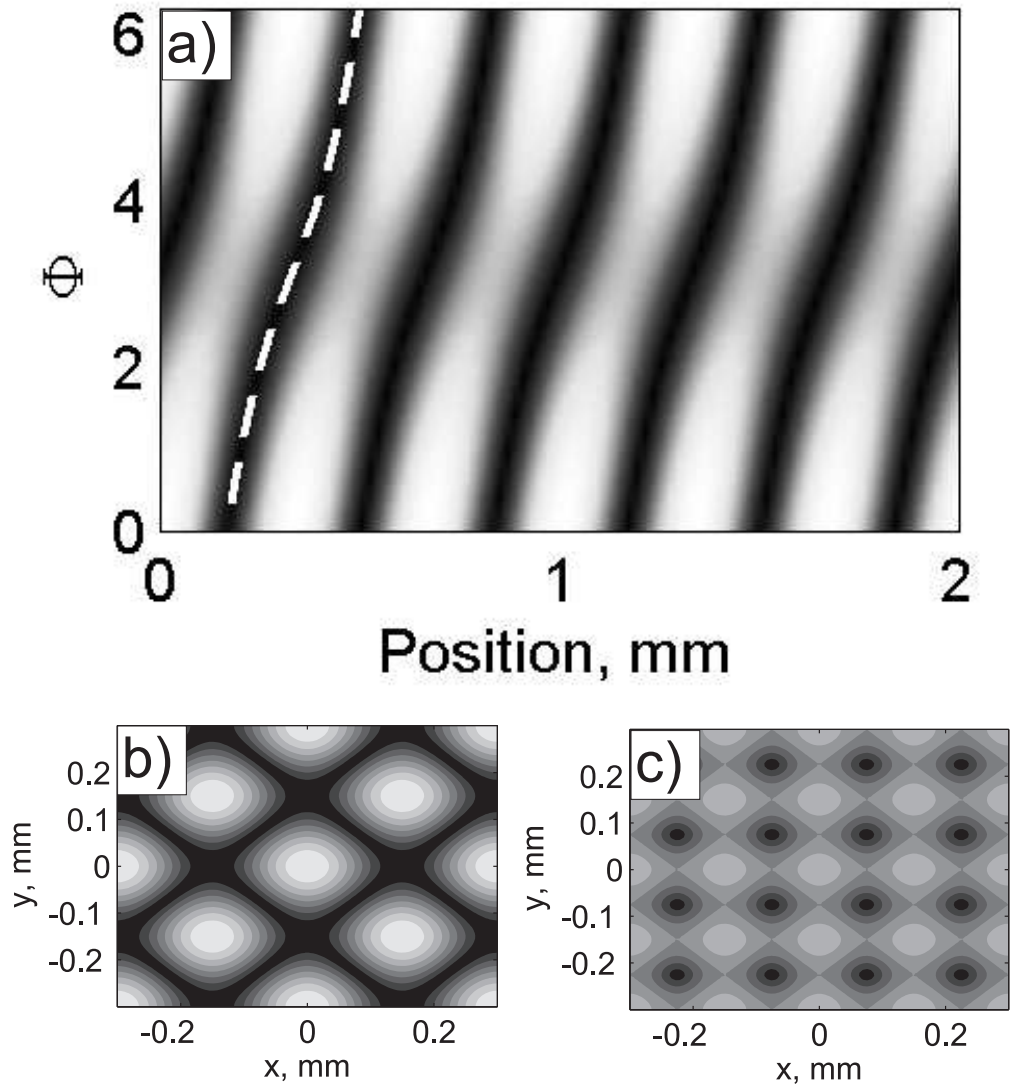

Figure 1. (a) Pressure amplitude for counter propagating planes waves from two opposing transducers with reflection coefficient, R =0.2, as a function of relative phase. Pressure calculated using equation 3.3. Dashed line is nodal position as given by equation 3.4. (b) Pressure amplitude for two orthogonal pairs of transducers in the absence of reflection, calculated using equation 3.8 with $\phi_1 = \phi_2 = \phi_3 = \phi_4 = 0$. (c) is as (a) but with $\phi_1 = \phi_2 = 0$ and $\phi_3 = \phi_4 = \pi/4$ so that equation 3.10 is satisfied. In (a) the plot is normalized such that the colour scale runs from black at 0 to white $2P_0$. In (b) and (c) the scale runs from black at 0 to white at $4P_0$

Each contribution has the same amplitude, P_0, but the phase delay applied to each, ϕ_n, can be varied independently. The total pressure can be written as the sum of these contributions:

$$\begin{aligned} P(x,y) &= P_1(x,y) + P_2(x,y) + P_3(x,y) + P_4(x,y) \\ &= 2P_0\Bigg[\exp\left(i\frac{\phi_1+\phi_2}{2}\right)\cos\left(kx+\frac{\phi_1-\phi_2}{2}\right) \\ &+ \exp\left(i\frac{\phi_3+\phi_4}{2}\right)\cos\left(ky+\frac{\phi_3-\phi_4}{2}\right)\Bigg]. \end{aligned} \tag{3.6}$$

Defining:

$$\begin{aligned} \phi_x &= \frac{\phi_1+\phi_2}{2} \\ \Delta\phi_x &= \phi_1-\phi_2 \\ \phi_y &= \frac{\phi_3+\phi_4}{2} \\ \Delta\phi_y &= \phi_3-\phi_4 \end{aligned} \tag{3.7}$$

equation 3.6 can be rewritten:

$$P(x,y) = 2P_0\left[\exp(i\phi_x)\cos\left(kx+\frac{\Delta\phi_x}{2}\right)+\exp(i\phi_y)\cos\left(ky+\frac{\Delta\phi_y}{2}\right)\right] \tag{3.8}$$

The aim is to be able to trap particles at pressure nodes, which can then be moved by changing the signals applied to the transducers. To this end it is necessary to calculate the positions and shapes of pressure nodes, which can most easily be achieved by calculating the modulus squared of the pressure in equation 3.8

$$\begin{aligned} |P(x,y)|^2 &= 4P_0^2\Big[\cos^2(kx+\Delta\phi_x/2)+\cos^2(ky+\Delta\phi_y/2) \\ &+ 2\cos(\phi_x-\phi_y)\cos(kx+\Delta\phi_x/2)\cos(ky+\Delta\phi_y/2)\Big]. \end{aligned} \tag{3.9}$$

If $\phi_x = \phi_y$ (as is the situation when $\phi_x = \phi_y = 0$ for example) then pressure nodes occur where $y = (2n-1)\frac{\lambda}{2} - \frac{\Delta\phi_x}{2k} - \frac{\Delta\phi_y}{2k} - x$ or $y = (2n-1)\frac{\lambda}{2} + \frac{\Delta\phi_x}{2k} - \frac{\Delta\phi_y}{2k} + x$. Although this indicates that there is a node pattern that can be shifted in the x and y directions by varying $\Delta\phi_x$ and $\Delta\phi_y$ the lack of any local trapping (the nodes form a grid of intersecting lines) limits the usefulness of this pattern. This pressure field can be seen in figure 1(b). More useful is the pattern, shown in figure 1(c), formed if the following relationship is obeyed:

$$\phi_y = \phi_x + \pi/2 \tag{3.10}$$

In that case the third term of equation 3.9 is zero and pressure nodes only occur where both $\cos^2(kx+\Delta\phi_x/2) = 0$ and $\cos^2(ky+\Delta\phi_y/2) = 0$. This leads of a

regular grid of traps (regions of zero pressure) at:

$$\begin{aligned} x &= (2n_x - 1)\frac{\lambda}{2} + \frac{\Delta\phi_x}{2\pi}\frac{\lambda}{2} \\ y &= (2n_y - 1)\frac{\lambda}{2} + \frac{\Delta\phi_y}{2\pi}\frac{\lambda}{2}. \end{aligned} \tag{3.11}$$

Where n_x and n_y are independent integers. The phase relationship in equation 3.10 and the resulting relationships between nodal positions and relative phases in equation 3.11 provide the basis for a method of manipulating particles in two dimensions. The following section describes the design of a practical device for realizing this.

4. Device design

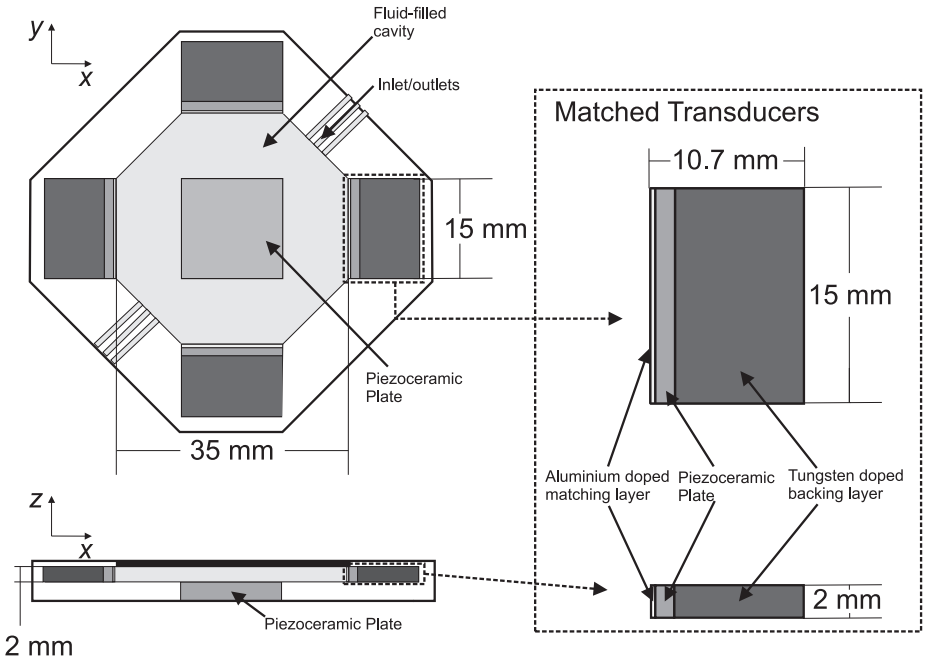

Figure 2. Schematic of device for manipulation of particles in two dimensions

In order to obtain manipulation in two dimensions two pairs of matched transducers are required, along with a single transducer, positioned on the base of the device in order to hold particles against gravity. The four manipulation transducers are designed to be acoustically matched to water (the fluid in the chamber) and include an absorbing backing. These features minimize the reflection of the incoming acoustic energy in order to reduce the standing waves produced by the reflections and ensure that the result of driving a single transducer is wave travelling away from the transducer. As demonstrated in section 3 counter propagating travelling waves can be used to produce a standing wave whose nodal

positions (which act as particle traps) are controlled by the phase of the excitation signals.

Matching layer performance is strongly dependent on frequency and so the transducers are designed for a specific frequency. In the frequency range in which existing analytical solutions are applicable (for particles much smaller than a wavelength) the acoustic radiation force increases linearly with frequency (Yosioka & Kawasima, 1955). Higher frequencies require higher tolerances in manufacture and so a compromise between manufacturing complexity and force is sought, and 5 MHz is selected as the operation frequency.

The device can be considered as three orthogonally arranged systems, the levitation system (arranged vertically) which lifts the particles and holds them in horizontal planes and then two manipulation stages which use the counter-propagating wave method to trap the particles in a grid of traps that can then be manipulated by altering the phases of the signals applied to the transducers.

The levitation stage consists of a straightforward resonant system consisting of a 15 mm $\times$ 15 mm piezoceramic plate of thickness 3 mm positioned 2 mm from a 1 mm thick microscope slide, which acts as a reflector. Application of a 5 MHz signal produces a standing wave with 13 nodes in the water-filled cavity between the piezoelectric plate front face and the reflector. The acoustic radiation force traps particles in layers at the nodes, allowing manipulation in the $x-y$ plane. The levitation transducer extends many (approximately 50) wavelengths in both the x- and y-directions and so the field is uniform (or at least very slowly varying in those directions), leading to forces (from the levitation field) directed only along the z-axis.

The four manipulation transducers are designed to minimize reflection in order to produce controllable fields, they consist of 2 mm $\times$ 15 mm $\times$ 1.3 mm thick piezoceramic plates with an alumina-loaded-epoxy matching layer applied to the front face and a tungsten-loaded-epoxy absorbing layer applied to the back face.

The matching layer is designed to minimize reflection by adding a layer with a thickness that is an odd-integer multiple of one quarter of the wavelength in the matching layer and an acoustic impedance of:

$$z_{\mathrm{m}} = \sqrt{z_{\mathrm{water}} z_{\mathrm{T}}} \tag{4.1}$$

where $z_{\mathrm{water}} = 1.5$ MRayl is the acoustic impedance of water and z_{T} is the acoustic impedance of the transducer material. For the NCE51 material used (a soft doped PZT material: Noliac group) the acoustic impedance is 35 MRayl and so equation 4.1 gives z_{m} =7.2 MRayl. This would require a very large concentration of alumina (in excess of the 30% by volume used by Wang et al. (2001)) in practice a more conservative approach was taken with 10% alumina by volume used, resulting in an acoustic impedance of 3.6 MRayl (Wang et al., 2001). In the following section, it is demonstrated using a one-dimensional acousto electric model that this leads to a reduction in reflection that is still sufficient to allow particle manipulation.

The aim of the backing layer is to ensure that all acoustic energy entering the transducer is absorbed. The absorption of tungsten doped epoxy peaks at 7.5% tungsten by volume, however the acoustic impedance increases with increasing tungsten content (Wang et al., 2001). A compromise value of 10% tungsten by volume was used, giving an absorption of 38 dB/mm (at 30 MHz) and an acoustic impedance of 5.6 MRayl (Wang et al., 2001). The backing layer was 9 mm thick.

Assuming that the attenuation varies linearly with frequency, as the tungsten particle radius (5 μm) is much smaller than one wavelength, then 99% of the acoustic energy should be absorbed in a single, 18 mm, roundtrip through the backing layer.

5. Modelling device behaviour

The analysis in section 3 described the behaviour of particles in a somewhat idealized manipulation system, but more involved models are required to assess the actual behaviour of the system shown in figure 2. Even considering the system as a one-dimensional system the reflection coefficient, R, and acoustic pressure amplitude need to be included to predict the behaviour of the system. To this end a one-dimensional electro-acoustic model was used to predict the behaviour of the particle trapping system. This, relatively straightforward, model allowed the study of design parameters (in particular the thickness of the component layers of the transducers) and prediction of the particle positions and trap strengths. The other major consideration in the assessment of the device design is the effect of the finite nature of the transducers on the resultant field, in particular in order to evaluate the region over which the particles can be effectively controlled and the pressure amplitude generated. This is addressed using a two-dimensional finite element model in section b.

(*a*) *One-dimensional electro-acoustic model*

The design of the manipulation system was analysed by a one dimensional electro-acoustic model, an approach similar to that previously used by Hill (2003) for the design of resonant devices. The system, including the fluid filled cavity, is modelled as a series of layers, infinite in the directions perpendicular to the wave propagation. Linear wave propagation is assumed through passive materials and an acousto-electric solution is used for the electrically active piezoelectric plates (Bui et al., 1977). The general approach is the same as the KLM equivalent circuit approach (Leedom et al., 1971) and a description of the method used here is given in Wilcox et al. (1998). The one dimensional model assumes that the dimensions perpendicular to the propagation direction are large compared to the wavelength. The system is 2 mm in the z-direction, which is 6.7 wavelengths at 5 MHz. This suggests that that this one-dimensional model will give only approximate results and a three-dimensional model would be required to fully model the device. However the one-dimensional model offers clear physical insights and the ability to perform rapid parameter studies to aid the design process.

Each layer is defined in terms of its thickness, d, cross-sectional area, A, acoustic impedance, Z, and Q-factor, Q, with piezoelectric layers also having a permittivity, ϵ and piezoelectric constant, $h_x x$. The piezoelectric coefficient is obtained from more readily available parameters by:

$$h_{xx} = k_t \sqrt{\frac{C^D_{xx}}{\epsilon}} \tag{5.1}$$

where k_t is the piezoelectric coupling coefficient, C^D_{xx} and is the open circuit stiffness in the direction of propagation (x).

The arrangement of the layers used to model the manipulation stage is shown in figure 3 and the material parameters are shown in table 1.

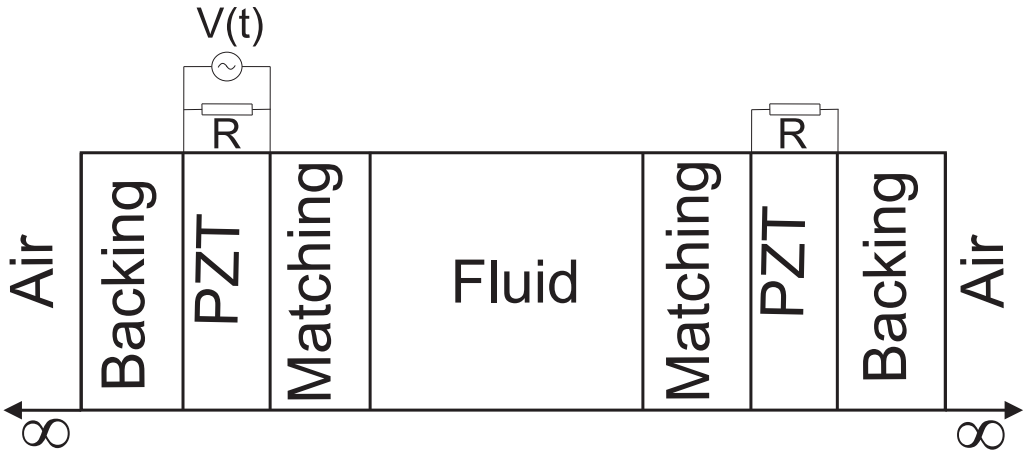

Figure 3. Ordering of layers in one-dimensional model, with electrical connection positions.

Using the one dimensional model to evaluate the reflection coefficient (as the ratio of waves propagating in the positive and negative x-directions in the fluid chamber under continuous excitation) allows the potential performance of the device to be assessed as a function of the material thicknesses and compositions.

Material	Thickness, d (mm)	Acoustic Impedance, Z (MRayl)	Q-factor, Q	Permittivity, ϵ	Piezoelectric coefficient, h_x ($\mathrm{Nm^{1/2}C^{-1}}$)
Air	∞	0.0004	∞		
Epoxy w. 10% W	9	5.6	11		
PCM51	1.33	35.1	80	1.6×10^{-8}	1.6×10^{9}
Epoxy w. 10% Al	0.4	3.6	19		
Water	35	1.5	100		

Table 1. Material parameters for components of manipulation stage

Figure 4 shows the reflection coefficient as a function of excitation frequency for the system described in figure 3 and table 1, but with the thickness of the matching layers on both transducers varied. It can be seen that there are two sources of reductions in the reflection coefficient: resonances either in the transducers or the matching layer. For this system the frequencies at which the former occur are mainly dependent on the transducer thickness, and are only weakly dependent of the matching layer thickness (and occur even where there is no matching layer). The matching layers behave as expected with reductions in reflection where the matching layer thickness is equal to an odd integer number of quarter wavelengths. Reflection can best be reduced by making these two frequencies coincident. For this reason, the transducer thickness (1.33 mm) was

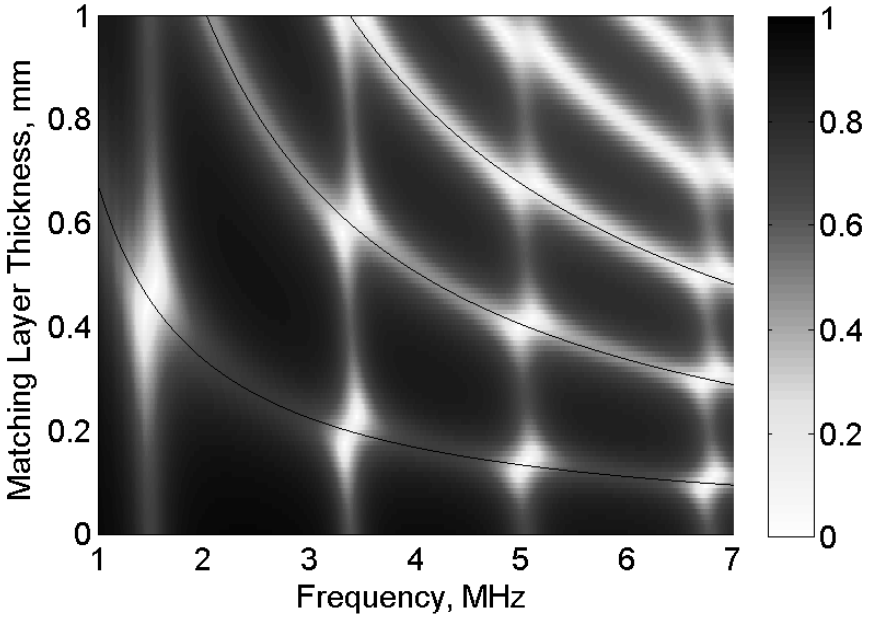

Figure 4. Reflection coefficient for transducers as function of frequency with varied matching layer thickness (calculated with one-dimensional electroacoustic model).

chosen to provide a resonance at 5 MHz and a matching layer thickness of 0.4 mm (3/4 λ at 5 MHz) was chosen to minimize reflection at 5 MHz.

The other key consideration is the pressure amplitude available. Figure 5 shows the pressure amplitude in the fluid cavity according to the one-dimensional electroacoustic model of the device with 0.4 mm matching layers. For each frequency the model is solved for an excitation of 30 V_{pp} and the resulting pressure peak in the cavity calculated. In addition to many peaks due to cavity resonances there are large peaks at 1.4 MHz and 5 MHz corresponding to resonances of the transducers. The excitation voltage is 30 V_{pp}, as used experimentally, and the peak pressure at 5 MHz is 300 kPa.

(*b*) *Two dimensional finite-element model*

The simplicity of the one dimensional model makes it well suited to studying the effect of varying experimental parameters, but it does not give the true field shape generated by orthogonal pairs of finite-sized transducers. In particular the positions of the nodes and the region over which particles can be trapped and manipulated is of interest.

(b.1) *The model*

A commercial finite-element package (PZFlex, Weidlinger Associates Inc.) was used to model the device described in section 4 in two dimensions with the direction perpendicular to the manipulation plane treated as plane strain. Square

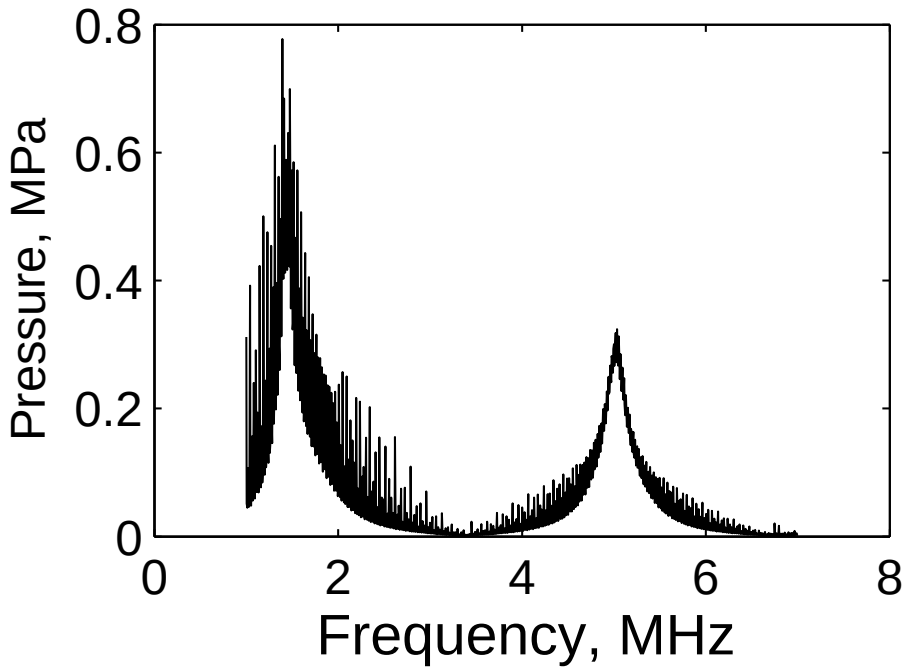

Figure 5. Peak pressure amplitude in the fluid cavity excited by single transducer, using 400 μm matching layers and an excitation voltage of 30 Vpp (calculated with one-dimensional electroacoustic model).

elements were used with 15 elements per wavelength and the model solved with an explicit time stepping solver. The geometry of the model is shown in figure 6. A symmetrical boundary condition is applied along the x axis to halve the size of the model. The remaining model boundaries have unconstrained boundary conditions.Two virtual experiments were undertaken. In the first a pulse of three cycles (with a top-hat envelope) at 5 MHz central frequency was applied and the incident and reflected pressure from a transducer was used to evaluate the reflection coefficient of the transducer. In the second experiment a continuous excitation at 5 MHz was applied until a steady state was achieved in order to evaluate the field shape of the device in operation. In each case the excitation was applied as a voltage across one of the transducers. The response to excitation of four transducers is calculated as a superposition of the solution for a single transducer, rotated appropriately.

(*c*) *Model Results*

Figure 7(a) shows the time domain signal for the pressure at the centre of the model system after a 3 cycle burst at 5MHz centre frequency has been applied across one of the transducers. Region (1) corresponds to the pulse passing the centre of the system directly from the input, and region (2) encompasses the first reflection from the opposing transducer. Figure 7 (b) shows the reflection coefficient calculated from the Fourier transforms of the two pulses (solid line)

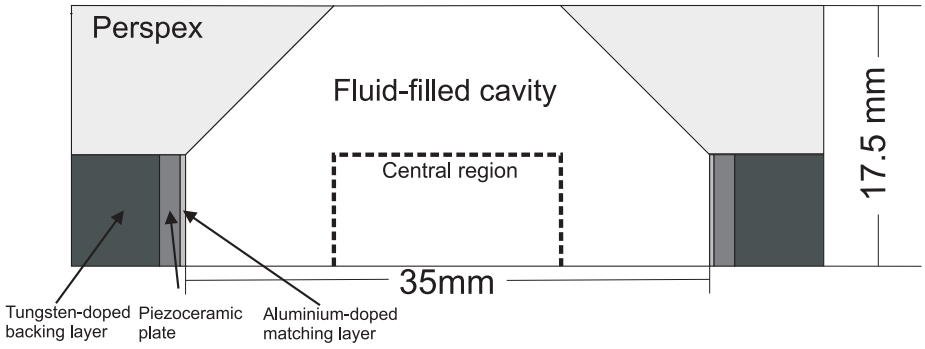

Figure 6. Top down view of two-dimensional finite-element model of device shown in figure 2.

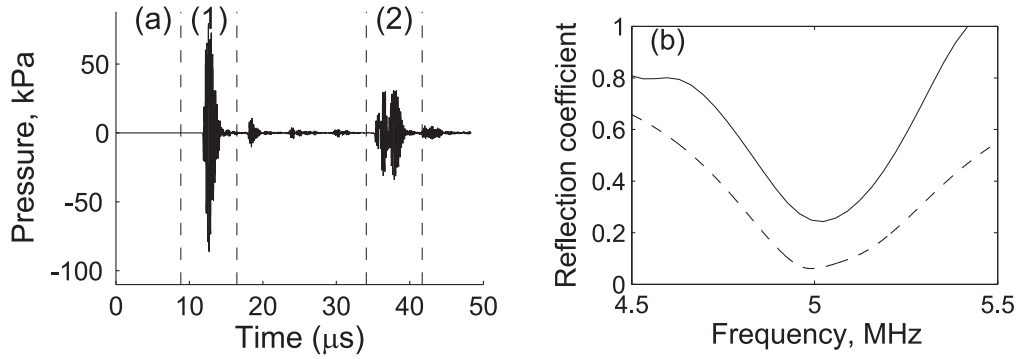

Figure 7. (a) Pressure at centre of device excited using 3 cycles of 5 MHz at 60 V_{pp}, calculated using FE model region (1) is incident wave and region (2) reflected. (b) Reflection coefficient calculated from Fourier transforms of incident and reflected pulses (solid line), with values calculated from one-dimensional model for comparison (dotted line).

and is shown compared to the reflection coefficient calculated using the one dimensional model.

Although the two dimensional model indicates a higher reflection coefficient than would be expected from the one-dimensional model, the value is still low enough to expect manipulation to be possible and the optimal operation frequency is unchanged at 5 MHz. The finite element model runs in the time domain, but running it with continuous sinusoidal excitation until a steady state is reached allows continuous single frequency excitation to be modelled effectively. Once a steady state is reached a fast Fourier transform is performed on the time response at each spatial point and the response at 5 MHz extracted. The pressure field, in terms of a complex amplitude field, in the fluid filled cavity resulting from continuous excitation at 5 MHz was calculated by this method and the response to simultaneous excitation by all four transducers was calculated as the sum of the calculated field rotated appropriately and with an independently variable phase applied to each contribution. Figure 8(a) shows the pressure amplitude in the central 15 mm $\times$ 15 mm region of the device (the region over the levitation stage)

and expanded images of the central 0.6 mm × 0.6 mm region are shown in (b) and (c). There is a consistent pressure across most of the region of interest (the area over the levitation transducer), with some amplitude reduction and distortion near the sides. The behaviour away from the edges is as predicted by equation 3.8. The application of phases such that $\Delta\phi_x = 0$,$\phi_x = 0$,$\Delta\phi_y = 0$ and $\phi_y = 0$, figures 8(a) and (b), gives a series of intersecting diagonal minima, making trapping difficult. In figure 8(c) the phase condition given in equation 3.10 is used and a regular grid of nodes is produced.

The pressure amplitudes in figure 8 are given per volt of excitation. For the excitation used experimentally (30 V_{pp}) the maximum pressure in the central region when $\Delta\phi_x = 0$, $\phi_x = 0$,$\Delta\phi_y = 0$ and $\phi_y = 0$, shown in figures 8(a) and (b)) is predicted to be 450 kPa. When $\Delta\phi_x = 0$, $\phi_x = 0$, $\Delta\phi_y = 0$ and $\phi_y = \pi/2$ the maximum pressure is 340 kPa. As can be seen in figure 8(c) these peaks occur on the diagonals of the traps. Of particular interest is the variation of pressure along the x- and y- directions passing through the traps, as this determines the force available for manipulation in those directions. In the central region this pressure varies sinusoidally with an amplitude of 225 kPa. Using this pressure, equations 2.1, 2.2 and 2.3 and the material parameters in table 2 can be used to predict a maximum force on 10-μm-diameter polystyrene spheres of 35 pN.

Material	Density, ρ kg/m^3	Bulk Modulus, K GPa
Polystyrene	1050	4.4
Water	997	2.2

Table 2. Material parameters used for calculation of force.

6. Experimental Results

Each of the five transducers was attached to a signal generator. The resonant nature of the levitation stage ensured that the signal direct from the generator (10 V_{pp} at 5MHz) was sufficient to trap 10 μm diameter polystyrene spheres against gravity. Without signal applied to the manipulation transducers the particles were randomly distributed across the region over the levitation transducer and appeared to move freely in the x-y plane, suggesting that any lateral forces resulting from the levitation stage are small. The 4 manipulation transducers (arranged in opposing pairs) require additional power amplification to provide voltages of 30 V_{pp}. The manipulation transducers were excited at 5 MHz in order to minimize reflection (see section 5) and each pair was synchronized to allow the relative phase of the excitations of the opposing transducers to be adjusted. The levitation stage is not synchronised with the manipulation transducers.

(*a*) *Trapping and manipulation*

Figure 9 shows the distribution of particles in a small region of the device, near the centre, for two operating conditions. In part (a) the transducer phases are adjusted to conform to equation 3.10 and trapping is achieved at a grid of

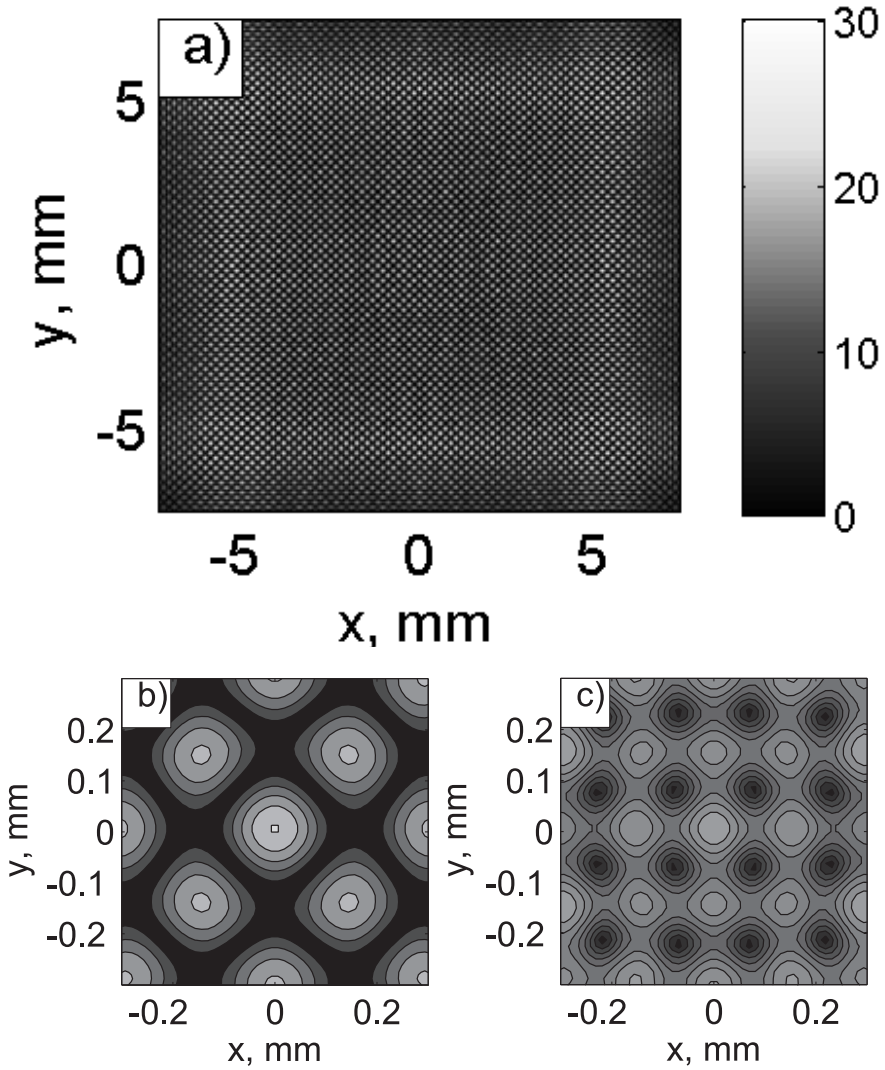

Figure 8. Pressure amplitude calculated using a 2D finite element model for the four transducer manipulation device excited at 5MHz. Color scale is pressure per applied volt in kPa. The phases of the four transducers are set to give $\Delta\phi_x = 0, \phi_x = 0, \Delta\phi_y = 0, \phi_y = 0$ for part (a). (a) is the central region marked in figure 6 (b) is an expanded view of the centre of the cavity. Part (c) is the expanded region, but with $\Delta\phi_x = 0, \phi_x = 0, \Delta\phi_y = 0, \phi_y = \pi/2$.

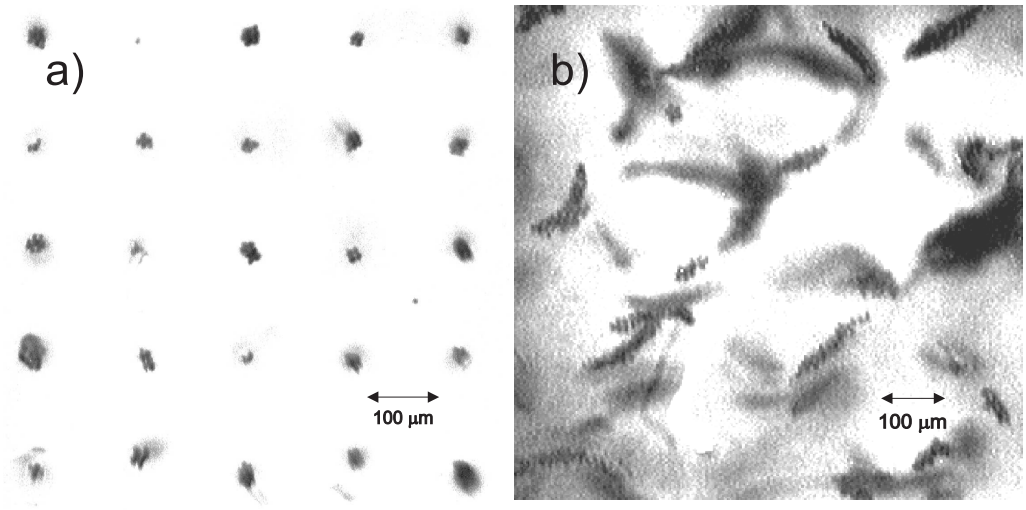

Figure 9. Photographs of 10 μm polystyrene beads near the centre of the device with 30 V_pp excitation at 5MHz: (a) transducer phases adjusted to obey equation 3.10; (b) transducers are all operated in phase.

points, as expected from the analytical result in equation 3.8. Part (b) shows the effect of running all four transducers in phase and, although poor trapping makes getting a good image difficult, particles can be seen to line up along diagonals as predicted analytically in section 3(b), see figure 1(b) for comparison, and by the FE model in section 5(c), figure 8(b).

Figure 10 shows the manipulation of agglomerates of particles in a single trap, the image is a composite of five images, with $\pi/2$ changes in $\Delta\phi_x$ and $\Delta\phi_y$ used to shift the trap position by $\lambda/8 = 38$ μm.

(*b*) *Device characterization*

In order to quantify the behaviour of the trap a series of images were produced varying the phase of the particle over a range $-2\pi \leq \Delta\phi_x \leq 2\pi$ in 36 steps and then the same for $-2\pi \leq \Delta\phi_y \leq 2\pi$. In each case the condition given in equation 3.10 is obeyed throughout. The images were used to determine the positions of the particle agglomerates as a function of phase using image tracking software (Crocker & Grier, 1996) Figures 11(a) and 11(b) show the relationship between position and phase for an agglomerate of particles when the relative phase of each pair of transducers is varied over a range of $-2\pi \leq \Delta\phi \leq 2\pi$. In each case the theoretical variation position, calculated from equation 3.4 is plotted, assuming a reflection coefficient of 0.06 as predicted by the one dimensional electro-acoustic model in section 5. The same equation is evaluated using an $R\cos(2kx_0)$ value determined with a least squares fit between the data and equation 3.4. For the variation of $\Delta\phi_x$ (i.e. the data in figure 11 (a)) the data appears to follow the expected result well and $R\cos(2kx_0) = 0.11$ is extracted from the least squares fit. Where $\Delta\phi_y$ is varied (in figures 11(c) and 11(d)) the measured position again follows equation 3.4, but the value of $R\cos(2kx_0)$ calculated is 0.33, higher than

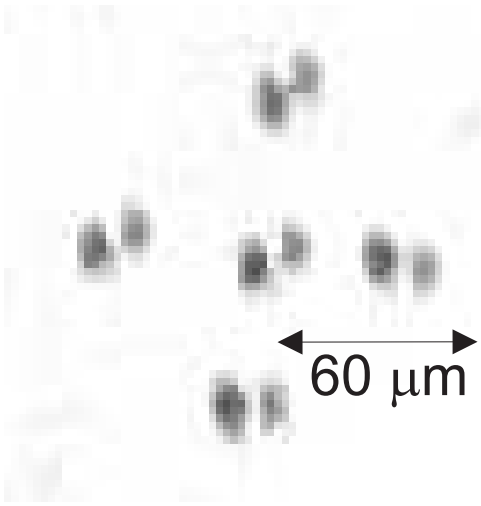

Figure 10. Composite of five images showing position of two particles, trapped in a single trap, initially with all four transducers synchronized according to equation 3.10 and then with additional phase delays of $\pm\pi/2$ applied across each pair of transducers in turn.

suggested by the 1D model. This suggests that one pair of transducers is less well matched than the other, but that the matching is still sufficient to allow manipulation of particles.

(*c*) *Force Calibration*

By changing, in a single step, $\Delta\phi_x$ by π the nodal position of the pressure field can be moved by $\lambda/4$. Observing the response of a particle to this change in field allows the amount of force to be evaluated. In a sinusoidal pressure field the force on the particle varies sinusoidally and the equation of motion, assuming a pressure node at $x = 0$, can be written:

$$m\ddot{x} = -F_0 \sin(2kx) - 6\pi\mu r\dot{x} \tag{6.1}$$

where F_0 is the maximum force (occurring at $x = \lambda = 80$ μm), r is the radius of the polystyrene sphere and μ is the dynamic viscosity of the fluid. Note that, although the viscosity can be neglected in the calculation of the acoustic radiation force, which results from the scattering of the acoustic wave, it can have a substantial effect on the motion of the particle in response to that force. If the system is overdamped then there is an analytical solution for the particle position:

$$x = \frac{1}{k}\arctan\left[\tan(kx_0)\exp\left(-\frac{kF_0}{3\pi\mu r}t\right)\right], \tag{6.2}$$

where x_0 is the initial position of the particle.

A node with a single trapped particle was selected and the response of the particle to a change of $\Delta\phi_x$ by π was recorded with a high speed camera at 92 fps and the particle position extracted using feature tracking software (Crocker & Grier, 1996). The change in position along the x axis is shown in figure 12. Also

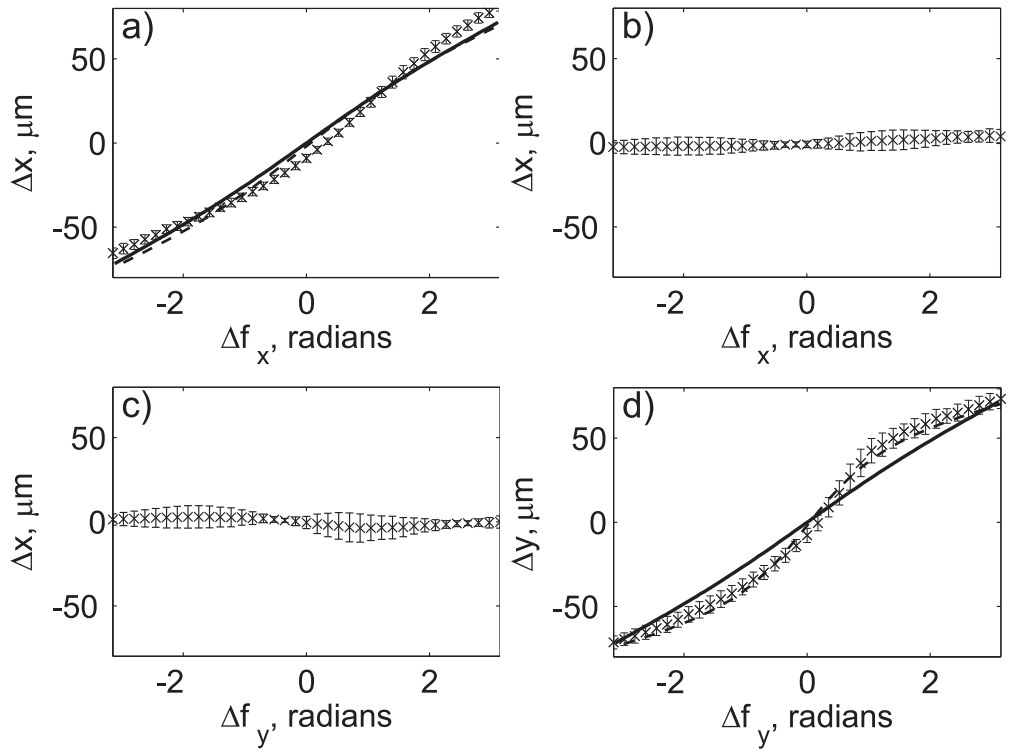

Figure 11. Position of trapped particles as a function of phase difference between, (a) and (b), transducers acting along x-axis and, (c) and (d), transducers acting along y-axis. In each case the crosses ($\times$) mark the change in position from the $\Delta\phi = 0$ position, averaged over 10 data sets. The error bars represent the standard deviation of the sets. The solid lines represent analytical results calculated from 3.4 using the reflection coefficient expected from the one dimensional model $R = 0.06$. The dashed lines represent analytical results withthe reflection coefficient chosen to minimize the mean square difference between the analytical result and the data.

shown is the trajectory given by equation 6.2 with F_0 evaluated by minimizing the root-mean-square error between the analytic response and the data. This approach indicates that in practice the maximum force generated is 30 pN, which is comparable to the value of 35 pN predicted using the finite-element model in section 5.

7. Scalable Implementation

Although it is possible to vary the field shape using four transducers, the variation is limited to moving between the field shapes shown in figure 1. Additional transducers would allow more flexible field control, however the fabrication approach of the device described previously makes construction of such prototypes time consuming. To alleviate this a scalable approach, allowing more rapid prototype development and arbitrary numbers of transducers, has

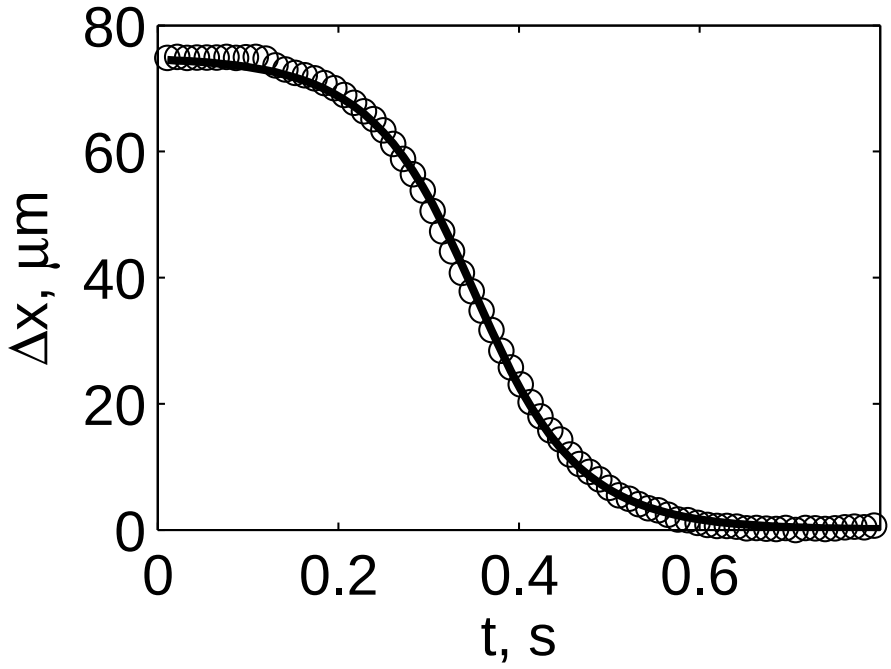

Figure 12. Path of 10 μm polystyrene sphere after changing $\Delta\phi_x$ by π. Circles are experimental values, solid line is solution to equation 6.2 with F_0 determined by root-mean-square-error minimization.

been investigated. The approach uses a flexible printed circuit board formed into a polygon to attach matched and backed transducers. To demonstrate that this is a viable approach it is shown that this method can be used to reproduce the technique of using four transducers to trap and manipulate polystyrene beads.

(*a*) *Device Description*

The transducers with alumina-doped matching layers are bonded to a flexible printed circuit board, or 'flex circuit' (Flexible dynamics Ltd, UK), and formed into an octagon. The octagonal flex circuit is first sandwiched between two Plexiglas plates to create a sealed unit. Then this sealed octagon is mounted on a rigid PCB to allow simple connection to each transducer element. Finally an alumina-doped absorbing backing is moulded to the back of the transducers. The device is shown schematically in figure 13(a), the depth of the fluid chamber is 10 mm. The piezoceramic plates were 5 mm $\times$ 5 mm with a thickness of 0.5 mm. The acoustic matching layer and absorbing backing have been designed to acoustically match the transducers to water and absorb the unwanted reflections, as in the previous device.

The flex circuit was a ribbon of 10 mm width and 80 mm length, each face of the octagon was 10 mm long. The eight transducers have a common ground. Four transducers (arranged in two orthogonal pairs) were each driven using a 4 MHz sine wave of 8 V_{pp}. Synchronization between channels was achieved

using two arbitrary waveform generators providing four outputs each allowing independent control of the amplitude, phase and frequency. The signals from the waveform generators were amplified by high speed buffers, BUF634T. The system is controlled by a virtual control panel developed in Labview that allows real time voltage, frequency and phase control. No levitation transducer is used for these tests, the rate of sedimentation of the beads is slow enough to allow trapping and manipulation without one. Adding a levitation transducer in the same configuration as before would be straightforward.

(*b*) *Key Results*

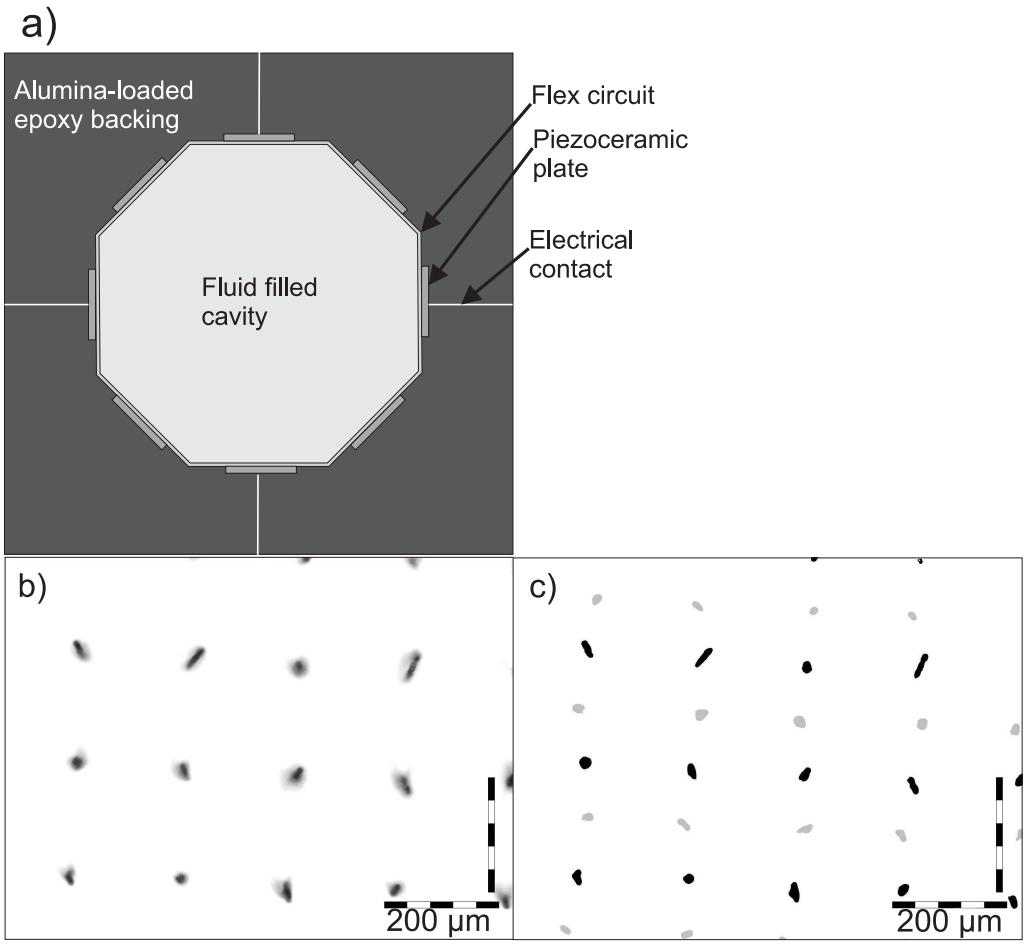

Figure 13. A scalable implementation of the manipulation device: (a) shows the device schematically (b) shows 10 μ-diameter particles trapped by exciting two orthogonal pairs of transducers and (c) is a composite image of the particles when the phase difference between two opposing transducers is 0 (black) and π (grey)

Four transducers, positioned as two orthogonal pairs in a manner analogous to the device described in section 4, were excited simultaneously and as a result

10 μm-diameter polystyrene beads were trapped on a grid with a nodal spacing of $\lambda/2$, as shown in figure 13(b). When the phase difference between opposing transducers is changed by π, the particles move with a distance of 94 μm ($\lambda/4$). This is demonstrated in Figure 13(c), which shows an overlay of pictures of the particles when the phase difference is 0 (in black) and when the phase difference is π (in grey).

8. Conclusions

A method of trapping and manipulating particles in two dimensions in fluid has been described, modelled and demonstrated. Pairs of opposing transducers, sufficiently well acoustically matched to the fluid and with an absorbing backing, allow a standing wave to be generated with nodal positions determined by the relative phases of the devices. It was shown analytically that imperfect matching leads to a divergence from the linear relation between phase difference and position, and introduces a variation in pressure amplitude with phase. The relationship between the phases of orthogonal pairs of transducers affects both the position and shape of nodes: the best approach for localized trapping and manipulation was derived. By considering each pair of transducers in terms of their phase difference and the arithmetic mean of their phases it is possible to trap particles at points by fixing the relationship between the mean phases of the two pairs, and then vary the trap position in each axis by adjusting the phase differences of the respective pairs. A manipulation device was designed and the effect of varying experimental parameters assessed using a one-dimensional electro-acoustic model. A two-dimensional finite-element model was used to predict the shape and amplitude of the field in the device. A device, consisting of a resonant levitation stage to hold particles against gravity and two pairs of acoustically matched transducers was constructed. Particle trapping and manipulation was demonstrated and behaviour was found to match that predicted analytically. The available force was determined by measuring the response of individual particles to a sudden change in the applied field. The force was found to be 30 pN for a 30 V_{pp} applied signal and this is in reasonable agreement with the value of 35 pN predicted from the finite-element model. An implementation using a flexible circuit material allowing the easy assembly of a variety of devices was demonstrated.

The ability demonstrated, to trap and freely manipulate particles in two-dimensions in an enclosed device represents, a significant step in the application of the acoustic radiation force, with potential implications for the biosciences.

Acknowledgment

This work was performed as part of the Sonotweezers project, funded by the EPSRC (Grant No. EP/G012067/1). The authors are grateful to their colleagues at the Institute for Medical Sciences and Technology (Dundee), for their aid in fabricating the transducers and to Weidlinger Associates for their assistance with the finite-element modelling.

References

Bui, L. N., Shaw, H. J., & Zitelli, L. T. (1977). Study of acoustic-wave resonance in piezoelectric pvf2 film. *IEEE Transactions On Sonics And Ultrasonics*, *24*(5), 331–336.

Coakley, W. T. (1997). Ultrasonic separations in analytical biotechnology. *Trends In Biotechnology*, *15*(12), 506–511.

Coakley, W. T., Hawkes, J. J., Sobanski, M. A., Cousins, C. M., & Spengler, J. (2000). Analytical scale ultrasonic standing wave manipulation of cells and microparticles. *Ultrasonics*, *38*(1-8), 638–641.

Courtney, C. R. P., Ong, C. K., Drinkwater, B. W., Wilcox, P. D., Demore, C., Cochran, S., Glynne-Jones, P., & Hill, M. (2010). Manipulation of microparticles using phase-controllable ultrasonic standing waves. *Journal Of The Acoustical Society Of America*, *128*(4), E195–E199.

Crocker, J. C., & Grier, D. G. (1996). Methods of digital video microscopy for colloidal studies. *Journal Of Colloid And Interface Science*, *179*(1), 298–310.

Demore, C., Glynne-Jones, P., Ye, C., Qiu, Y., Anderson, A., Hill, M., & Cochran, S. (2010). Transducer arrays for ultrasonic particle manipulation. In *IEEE International Ultrasonics Symposium 2010*, IEEE International Ultrasonics Symposium Proceedings. San Diego, CA, USA: IEEE. In Press.

Doinikov, A. A. (1994). Acoustic radiation pressure on a rigid sphere in a viscous-fluid. *Proceedings Of The Royal Society Of London Series A-Mathematical And Physical Sciences*, *447*(1931), 447–466.

Doinikov, A. A. (1996). On the radiation pressure on small spheres. *Journal Of The Acoustical Society Of America*, *100*(2), 1231–1233.

Doinikov, A. A. (1997). Acoustic radiation force on a spherical particle in a viscous heat-conducting fluid.1. general formula. *Journal Of The Acoustical Society Of America*, *101*(2), 713–721.

Glynne-Jones, P., Boltryk, R. J., Harris, N. R., Cranny, A. W. J., & Hill, M. (2010). Mode-switching: A new technique for electronically varying the agglomeration position in an acoustic particle manipulator. *Ultrasonics*, *50*(1), 68–75.

Gor'kov, L. (1962). On the forces acting on a small particle in an acoustical field in an ideal fluid. *Soviet Physics - Doklady*, *6*, 773–775.

Haake, A., & Dual, J. (2002). Micro-manipulation of small particles by node position control of an ultrasonic standing wave. *Ultrasonics*, *40*(1-8), 317–322.

Hill, M. (2003). The selection of layer thicknesses to control acoustic radiation force profiles in layered resonators. *Journal Of The Acoustical Society Of America*, *114*(5), 2654–2661.

Johnson, D. A., & Feke, D. L. (1995). Methodology for fractionating suspended particles using ultrasonic standing wave and divided flow fields. *Separations Technology*, *5*(4), 251–258.

King, L. (1934). On the acoustic radiation pressure on spheres. *Proceedings of the Royal Society of London, Series A*, *147*(861), 212–240.

Kozuka, T., Tuziuti, T., Mitome, H., & Fukuda, T. (1996). Acoustic micromanipulation using a multi-electrode transducer. In *7th International Symposium on Micro Machine and Human Science*, (pp. 163–170). Nagoya, Japan.: IEEE.

Kozuka, T., Tuziuti, T., Mitome, H., & Fukuda, T. (1998a). Control of a standing wave field using a line-focused transducer for two-dimensional manipulation of particles. *Japanese Journal Of Applied Physics Part 1-Regular Papers Short Notes & Review Papers*, *37*(5B), 2974–2978.

Kozuka, T., Tuziuti, T., Mitome, H., Fukuda, T., & Arai, F. (1998b). Control of position of a particle using a standing wave field generated by crossing sound beams. In *1998 IEEE Ultrasonics Symposium - Proceedings, Vols 1 And 2*, Ultrasonics Symposium, (pp. 657–660). New York: IEEE.

Kundt, A. (1868). Acoustic experiments. *Philosphical Magazine*, *4*(35), 41–48.

Kwiatkowski, C. S., & Marston, P. L. (1998). Resonator frequency shift due to ultrasonically induced microparticle migration in an aqueous suspension: Observations and model for the maximum frequency shift. *Journal Of The Acoustical Society Of America*, *103*(6), 3290–3300.

Laurell, T., Petersson, F., & Nilsson, A. (2007). Chip integrated strategies for acoustic separation and manipulation of cells and particles. *Chemical Society Reviews*, *36*(3), 492–506.

Lee, J., Ha, K., & Shung, K. K. (2005). A theoretical study of the feasibility of acoustical tweezers: Ray acoustics approach. *Journal Of The Acoustical Society Of America*, *117*(5), 3273–3280.

Lee, J., & Shung, K. K. (2006). Radiation forces exerted on arbitrarily located sphere by acoustic tweezer. *Journal Of The Acoustical Society Of America*, *120*(2), 1084–1094.

Lee, J., Teh, S. Y., Lee, A., Kim, H. H., Lee, C., & Shung, K. K. (2009). Single beam acoustic trapping. *Applied Physics Letters*, *95*(7), 073701.

Leedom, D. A., R, K., & Matthaei, G. L. (1971). Equivalent circuits for transducers having arbitrary even-symmetry or odd-symmetry piezoelectric excitation. *IEEE Transactions On Sonics And Ultrasonics*, *SU18*(3), 128–141.

Marston, P. L. (2006). Axial radiation force of a bessel beam on a sphere and direction reversal of the force. *Journal Of The Acoustical Society Of America*, *120*(6), 3518–3524.

Min, S. L., Holt, R. G., & Apfel, R. E. (1992). Simulation of drop dynamics in an acoustic positioning chamber. *Journal Of The Acoustical Society Of America*, *91*(6), 3157–3165.

Mitri, F. G. (2008). Acoustic radiation force on a sphere in standing and quasi-standing zero-order bessel beam tweezers. *Annals Of Physics*, *323*(7), 1604–1620. ISI Document Delivery No.: 317BS Times Cited: 21 Cited Reference Count: 83 English Article 0003-4916.

Mitri, F. G. (2009). Acoustic radiation force of high-order bessel beam standing wave tweezers on a rigid sphere. *Ultrasonics*, *49*(8), 794–798.

Mitri, F. G. M. F. G., Garzon, F. H., & Sinha, D. N. (2011). Characterization of acoustically engineered polymer nanocomposite metamaterials using x-ray microcomputed tomography. *Review Of Scientific Instruments*, *82*(3).

Pamme, N. (2007). Continuous flow separations in microfluidic devices. *Lab On A Chip*, *7*(12), 1644–1659.

Saito, M., Daian, T., Hayashi, K., & Izumida, S. (1998). Fabrication of a polymer composite with periodic structure by the use of ultrasonic waves. *Journal Of Applied Physics*, *83*(7), 3490–3494.

Saito, M., Itagaki, K., Hayashi, K., & Tsubata, K. (1999). Composite materials with ultrasonically induced layer or lattice structure. *Japanese Journal Of Applied Physics Part 1-Regular Papers Short Notes & Review Papers*, *38*(5B), 3028–3031.

Shi, J. J., Ahmed, D., Mao, X., Lin, S. C. S., Lawit, A., & Huang, T. J. (2009). Acoustic tweezers: patterning cells and microparticles using standing surface acoustic waves (ssaw). *Lab On A Chip*, *9*(20), 2890–2895.

Trinh, E., Robey, J., Jacobi, N., & Wang, T. (1986). Dual-temperature acoustic levitation and sample transport apparatus. *Journal Of The Acoustical Society Of America*, *79*(3), 604–612.

Wang, H. F., Ritter, T., Cao, W. W., & Shung, K. K. (2001). High frequency properties of passive materials for ultrasonic transducers. *IEEE Transactions On Ultrasonics Ferroelectrics And Frequency Control*, *48*(1), 78–84.

Wilcox, P. D., Monkhouse, R. S. C., Cawley, P., Lowe, M. J. S., & Auld, B. A. (1998). Development of a computer model for an ultrasonic polymer film transducer system. *Ndt & E International*, *31*(1), 51–64.

Wood, C. D., Cunningham, J. E., O'Rorke, R., Walti, C., Linfield, E. H., Davies, A. G., & Evans, S. D. (2009). Formation and manipulation of two-dimensional arrays of micron-scale particles in microfluidic systems by surface acoustic waves. *Applied Physics Letters*, *94*(5).

Wood, C. D., Evans, S. D., Cunningham, J. E., O'Rorke, R., Walti, C., & Davies, A. G. (2008). Alignment of particles in microfluidic systems using standing surface acoustic waves. *Applied Physics Letters*, *92*(4).

Wu, J. R. (1991). Acoustical tweezers. *Journal Of The Acoustical Society Of America*, *89*(5), 2140–2143.

Wu, J. R., & Du, G. H. (1990). Acoustic radiation force on a small compressible sphere in a focused beam. *Journal Of The Acoustical Society Of America*, *87*(3), 997–1003.

Yamakoshi, Y., & Noguchi, Y. (1998). Micro particle trapping by opposite phases ultrasonic travelling waves. *Ultrasonics*, *36*(8), 873–878.

Yasuda, K., Umemura, S., & Takeda, K. (1995). Concentration and fractionation of small particles in liquid by ultrasound. *Japanese Journal Of Applied Physics Part 1-Regular Papers Short Notes & Review Papers*, *34*(5B), 2715–2720.

Yosioka, K., & Kawasima, Y. (1955). Acoustic radiation pressure on a compressible sphere. *Acustica*, *5*, 167–173.